CAUCHY – Jurnal Matematika Murni dan Aplikasi
Volume 11 (2) (2026), Pages 1844–1866
p-ISSN: 2086-0382; e-ISSN: 2477-3344

SVIR Model Analysis of Measles with Incomplete Vaccination and Waning Immunity: Sidoarjo-Indonesia Case

Ainishafa, Abadi*, and Dian Savitri

Magister Matematika Study Program, The Faculty of Mathematics and Natural Science, Universitas Negeri Surabaya, Indonesia

Abstract

Measles remains a significant public health challenge in Indonesia. Sidoarjo City, despite reporting relatively high aggregate vaccination coverage, has experienced recurrent outbreaks, motivating a closer dynamical analysis of transmission risk under imperfect and waning vaccine-induced immunity. This study develops and analyzes a SVIR compartmental model for measles transmission in Sidoarjo City, Indonesia, incorporating waning immunity. The basic reproduction number $\mathcal{R}_0$ is derived using the next-generation matrix method, and the global stability of both the disease-free and endemic equilibria is rigorously proven via Lyapunov functions. Model parameters are estimated from weekly 2023 surveillance data in Sidoarjo City using Particle Swarm Optimization (PSO), Extended Kalman Filter, Maximum Likelihood Estimation, and Least Squares, and evaluated via MAPE. PSO achieves the lowest MAPE (10.82%), outperforming the other methods. The estimated $\mathcal{R}_0 = 0.668$ confirms a disease-free regime. Normalized sensitivity analysis identifies vaccine efficacy as the most influential parameter; a decline in efficacy to 0.75 elevates $\mathcal{R}_0$ close to the critical threshold, and any further reduction pushes the system into an endemic state. These findings underscore the necessity of maintaining high vaccine efficacy through completion of the two-dose routine immunization schedule (MCV1/MCV2) and supplementary immunization activities (SIA) and strengthened immunization strategies to sustain measles elimination at the district level.

Keywords: SVIR model ; measles ; waning immunity ; basic reproduction number ; particle swarm optimization ; sensitivity analysis

Copyright © 2026 by Authors, Published by CAUCHY Group. This is an open access article under the CC BY-SA License (https://creativecommons.org/licenses/by-sa/4.0)

1. Introduction

Measles, caused by the *Morbillivirus*, remains a serious and persistent threat to global public health, particularly in low- and middle-income countries where immunization coverage is uneven or suboptimal. Despite the availability of a highly effective vaccine for several decades, the disease continues to cause more than 100,000 deaths annually worldwide, the vast majority of which occur among children under five years of age [1]. In Indonesia, the magnitude of the problem remains considerable: the Ministry of Health recorded more than 6,000 confirmed cases and 104 deaths in 2024 alone, with incidence concentrated in regions with low routine immunization coverage [2]. Sidoarjo City, East Java, Indonesia characterized by high population mobility and heterogeneous vaccination coverage across its districts serves as a particularly instructive setting for examining the local dynamics of measles transmission. Beyond gaps in vaccination coverage,

*Corresponding author. E-mail: abadi@unesa.ac.id

Received: June 15, 2026 Revised: July 21, 2026 Accepted: August 7, 2026
DOI: https://doi.org/10.18860/cauchy.v11i2.43842

two biological factors further complicate control efforts: *waning immunity*, whereby vaccine-induced protection diminishes over time, and primary vaccine failure, in which a proportion of vaccinated individuals never mount a sufficient immune response [3, 4]. These factors underscore the inadequacy of relying solely on routine immunization programs and motivate the need for quantitative frameworks capable of characterizing transmission risk and informing evidence-based policy to sustain measles elimination.

Although two-dose measles vaccination generally provides long-lasting protection, primary vaccine failure and individual variation in immune response may leave a small proportion of vaccinated individuals susceptible to infection [5]. Therefore, the $V \to S$ transition in this study represents a phenomenological effective loss of protection at the population level rather than the assumption that measles vaccine-induced immunity universally disappears after a fixed period. Mathematical modeling has become an indispensable tool in epidemiology for understanding disease transmission dynamics and evaluating the impact of intervention strategies [6, 7]. The foundational SIR framework of Kermack and McKendrick [8] partitions the population into susceptible, infectious, and recovered compartments, providing a tractable basis for theoretical analysis; however, it does not explicitly represent the vaccinated subpopulation or account for the imperfect and time-limited nature of vaccine-induced immunity. To overcome these limitations, the *Susceptible–Vaccinated–Infected–Recovered* (SVIR) model introduces a dedicated vaccination compartment V, enabling explicit representation of both imperfect vaccination and waning immunity [9, 10]. Recent work by Fakhruddin et al. [11] demonstrated the applicability of the SVIR framework to measles in an Indonesian urban context (Jakarta), establishing local stability conditions and conducting numerical simulations from surveillance data; nevertheless, several analytical and methodological gaps remain unaddressed. First, rigorous proof of *global* asymptotic stability for both the disease-free and endemic equilibria of the SVIR model with waning immunity has received limited attention, with most studies restricting their analysis to local stability via linearization [10, 12]. Second, parameter estimation for such models is typically performed using a single computational method, leaving the comparative performance of alternative approaches largely unexplored; third, district-level analyses of measles dynamics in Indonesia integrating analytical results with locally calibrated simulations remain scarce relative to national and provincial studies.

The present study addresses these gaps through a comprehensive dynamical-systems analysis of the SVIR model applied to measles transmission in Sidoarjo City, East Java, Indonesia. Specifically, this study pursues five objectives. First, it constructs a biologically motivated SVIR model incorporating waning vaccine-induced immunity and natural demographic turnover. Second, it derives analytical expressions for the basic reproduction number $\mathcal{R}_0$ and the system's equilibrium points. Third, it rigorously proves the local and global asymptotic stability of both the disease-free equilibrium (DFE) and the endemic equilibrium (EE) via Jacobian linearization and Lyapunov function approaches, respectively. Fourth, it estimates model parameters from weekly measles surveillance data recorded in Sidoarjo City in 2023 using four computational methods: Particle Swarm Optimization (PSO), Extended Kalman Filter (EKF), Maximum Likelihood Estimation (MLE), and Least Squares (LS) which evaluated via Mean Absolute Percentage Error (MAPE); fifth, it performs numerical simulations using the best-fitting parameter set and conducts a normalized sensitivity analysis of $\mathcal{R}_0$ to identify the parameters most critical for disease control.

The principal contributions of this study are threefold. First, while Yang et al. [13] established global stability for a general SVIR framework, their model does not incorporate an explicit waning-immunity transition ($V \to S$) calibrated to empirical incidence data, and Fakhruddin et al. [11] calibrated an SVIR model to Jakarta data but restricted stability analysis to local linearization; the present study addresses both gaps by combining explicit waning immunity with complete global stability proofs. Second, we introduce a systematic, four-method parameter estimation framework with quantitative comparison, offering a more rigorous calibration approach

than those employed in existing SVIR studies, including the Jakarta-based analysis of Fakhruddin et al. [11], and yielding a reproducible benchmark for future modeling work in similar settings. Third, we deliver the first district-level dynamical analysis of measles in Sidoarjo City, East Java, Indonesia, translating theoretical results into practically interpretable findings for local public health authorities.

The remainder of this paper is organized as follows. Section 2 presents the model formulation, equilibrium analysis, stability proofs, parameter estimation methods, and sensitivity analysis framework. Section 3 reports the analytical and numerical results, including the estimated parameter values, the value of $\mathcal{R}_0$, and the sensitivity indices. Section 3 interprets the findings in their epidemiological context and discusses their implications for measles control policy in Sidoarjo City, East Java, Indonesia. Section 5 summarizes the main conclusions and outlines directions for future research.

2. Methods

This study employs a mathematical modeling approach to investigate measles transmission dynamics, adopting the *Susceptible–Vaccinated–Infected–Recovered* (SVIR) framework, which partitions the population into susceptible (S), vaccinated (V), infectious (I), and recovered (R) compartments. The model modifies previous compartmental frameworks by incorporating vaccination and vaccine-induced waning immunity as critical factors in measles control, and assumes a homogeneously mixed population at the city level; sub-district heterogeneity in vaccination coverage is not explicitly modeled and is discussed as a limitation in Section 5.

Based on a systematic literature review of measles epidemiology and SVIR-type models [13, 14], three modifications align the model with measles' biological characteristics: (1) a vaccination rate transitioning $S \to V$; (2) waning immunity, whereby vaccinated individuals return to S at a fixed rate [15]; and (3) natural birth and death rates in every compartment, reflecting an open population. These assumptions are formulated as an autonomous ODE system.

The mathematical analysis proceeds in four steps. First, the Disease-Free Equilibrium (DFE) and endemic equilibrium are obtained by setting all derivatives to zero. Second, the basic reproduction number $\mathcal{R}_0$ is computed via the next-generation matrix method, $\mathcal{R}_0 = \rho(FV^{-1})$, where F and V denote the new-infection and transfer-rate matrices evaluated at the DFE [16]. Third, local stability is assessed via Jacobian linearization, with negative real parts of all eigenvalues implying local asymptotic stability [17]. Fourth, global asymptotic stability of both equilibria is established via Lyapunov functions, fully characterized in terms of $\mathcal{R}_0$ [13, 18].

Model parameters are estimated from weekly 2023 measles incidence data for Sidoarjo City using four methods: PSO, EKF, MLE, and LS — chosen for their distinct strengths in handling nonlinear ODE systems [19–21]. PSO iteratively minimizes model-data discrepancy via swarm-based search [19]; EKF recursively estimates states and parameters jointly via first-order Taylor linearization [20]; MLE maximizes the likelihood of observed data under the model, and LS minimizes squared residuals [21]. Performance is compared via Mean Absolute Percentage Error (MAPE),

$$\text{MAPE} = \frac{1}{n}\sum_{t=1}^{n}\left|\frac{y_t - \hat{y}_t}{y_t}\right| \times 100\%, \tag{1}$$

where y_t, $\hat{y}_t$, and n denote the observed value, predicted value, and number of observations, respectively; the method with the lowest MAPE is selected for all subsequent analyses.

Using the best-fitting parameters, a normalized sensitivity analysis of $\mathcal{R}_0$ [15] is conducted,

$$\Upsilon_p^{\mathcal{R}_0} = \frac{\partial \mathcal{R}_0}{\partial p} \times \frac{p}{\mathcal{R}_0}, \tag{2}$$

where a positive (negative) index indicates $\mathcal{R}_0$ increases (decreases) with parameter p, identifying which parameters most strongly drive transmission and thus warrant prioritized intervention.

Finally, numerical simulations using the optimal parameters illustrate each compartment's temporal evolution, interpreted for epidemiological significance. All computations were performed in MATLAB using the fourth-order Runge–Kutta ODE solver.

2.1. Computational Implementation Details

To ensure reproducibility, this subsection reports the objective function, algorithm settings, initial conditions, and state-space specifications used across the four estimation methods.

All methods estimate $\theta = (\beta, \gamma, \xi, \sigma)$ by fitting the model-predicted weekly incidence $I(t;\theta)$ against observed surveillance data. For PSO and LS, the objective function is

$$J(\theta) = \sum_{t=1}^{n} \left(\frac{I(t;\theta) - I_{obs}(t)}{I_{obs}(t)} \right)^2, \tag{3}$$

where $I(t;\theta)$ solves system (3)–(6) via fourth-order Runge–Kutta with initial conditions $S(0) = 999{,}800$, $V(0) = 100$, $I(0) = 200$, $R(0) = 0$ (consistent with $N = 1{,}000{,}000$ in Table 1), and $I_{obs}(t)$ is the observed weekly case count, $t = 1, \ldots, 52$. For MLE, weekly cases are assumed Poisson-distributed with mean $I(t;\theta)$, and θ is estimated by maximizing the corresponding log-likelihood via `fmincon`. For EKF, θ is appended to the state vector and estimated recursively as new observations arrive.

PSO minimizes Eq. (3) using a swarm of 40 particles, inertia weight $w = 0.7$, cognitive and social coefficients $c_1 = c_2 = 1.5$, and a maximum of 200 iterations (Table 1).

Table 1: PSO algorithm settings.

Setting	Value
Swarm size	40
Maximum iterations	200
Inertia weight (w)	0.7
Cognitive coefficient (c_1)	1.5
Social coefficient (c_2)	1.5

The EKF augments the state vector as $x_t = (S_t, V_t, I_t, R_t, \beta_t, \gamma_t, \xi_t, \sigma_t)^\top$ under a random-walk parameter model $\theta_{t+1} = \theta_t + w_t$, with discrete-time transition

$$x_{t+1} = f(x_t) + w_t, \qquad y_t = Hx_t + v_t, \tag{4}$$

where $f(\cdot)$ discretizes (3)–(6) via Euler's method ($\Delta t = 1$ week), $H = [0, 0, 1, 0, 0, 0, 0, 0]$ selects I_t, and $w_t \sim \mathcal{N}(0, Q)$, $v_t \sim \mathcal{N}(0, R_{noise})$ with

$$Q = 10^{-5}\, I_{n_x+n_p}, \qquad R_{noise} = 10^{-4}. \tag{5}$$

The Jacobian of f is recomputed at each time step for the standard EKF covariance propagation and update [20]. LS minimizes Eq. (3) directly via `lsqnonlin`.

3. Results and Discussion

This section develops and analyzes the proposed SVIR measles model for Sidoarjo City, East Java, in five stages: model construction, equilibrium and basic reproduction number derivation, local and global stability analysis (via Jacobian linearization and Lyapunov functions), parameter estimation from 2023 Sidoarjo surveillance data with sensitivity analysis of R_0, and numerical simulation validating the analytical results.

3.1. Model Construction

The SVIR model partitions the total population N into *Susceptible* (S), *Vaccinated* (V), *Infected* (I), and *Recovered* (R) compartments, assuming a constant population (birth rate Λ balances

natural death rate μ). Susceptibles are vaccinated at rate ξ; since vaccine efficacy $\varepsilon \in (0, 1)$ is imperfect, vaccinated individuals remain infected with probability $(1 - \varepsilon)$, and immunity wanes at rate σ, returning V to S. Transmission follows mass action with rate β; infected individuals recover at rate γ, acquiring permanent immunity. Disease-induced death is neglected as negligible. The population is assumed homogeneously mixed at the city level; sub-district heterogeneity in vaccination coverage is not modeled and is discussed as a limitation in Section 5.

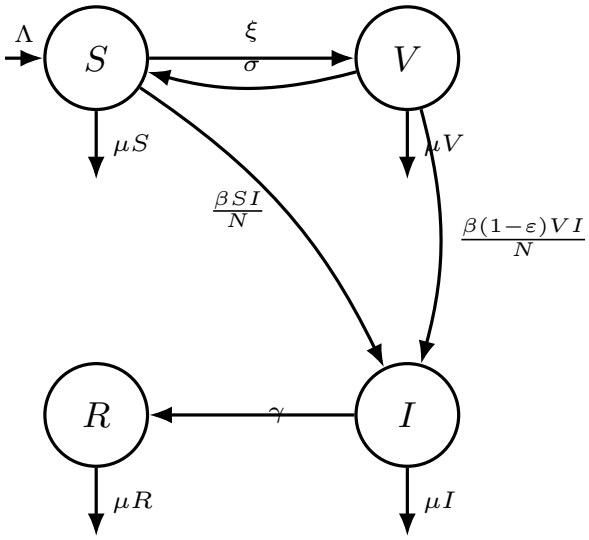

Fig. 1: Flowchart of the SVIR model with *waning immunity*.

Based on the diagram in Figure 1, the dynamics of disease spread are formulated into the following system of nonlinear ordinary differential equations:

$$\frac{dS}{dt} = \Lambda - \frac{\beta SI}{N} - (\mu + \xi)S + \sigma V \tag{6}$$

$$\frac{dV}{dt} = \xi S - \frac{(1-\varepsilon)\beta VI}{N} - (\mu + \sigma)V \tag{7}$$

$$\frac{dI}{dt} = \frac{\beta SI}{N} + \frac{(1-\varepsilon)\beta VI}{N} - (\gamma + \mu)I \tag{8}$$

$$\frac{dR}{dt} = \gamma I - \mu R \tag{9}$$

where $N = S + V + I + R$. All parameters are positive and $\varepsilon \in (0, 1)$. This system is analyzed in the feasible region $\Omega = \{(S, V, I, R) \in \mathbb{R}^4_+ : S + V + I + R = N\}$.

3.2. Model Parameters

Model parameters consist of fixed parameters obtained from the literature and demographic data, as well as parameters estimated from the data, both summarized in Table 2.

Table 2: Parameters of the SVIR model.

Parameter	Symbol	Value
Natural death rate	μ	2.75×10^{-4}
Vaccine effectiveness	ε	0.85
Birth rate	Λ	μN
Total population	N	1,000,000
Transmission rate	β	Estimated
Recovery rate	γ	Estimated
Vaccination rate	ξ	Estimated
Immunity waning rate	σ	Estimated

3.3. Basic Reproduction Number (R_0)

The basic reproduction number R_0 is calculated using the *next-generation matrix* method [12]. In the model Eq. (6)–Eq. (9), the only compartment involved in the transmission chain is I, so the vector of the rate of new infections $\mathcal{F}$ and the vector of the outflow rate from the infection compartment $\mathcal{V}$ are defined as

$$\mathcal{F} = \frac{\beta S I}{N} + \frac{(1-\varepsilon)\beta V I}{N}, \tag{10}$$

$$\mathcal{V} = (\gamma + \mu + \alpha) I, \tag{11}$$

where α represents the disease mortality rate. In this study, $\alpha = 0$ because the fatality rate of measles is very low. However, this parameter is still included to preserve the general form of the equations.

Evaluating the Jacobian matrices of $\mathcal{F}$ and $\mathcal{V}$ with respect to I at the disease-free equilibrium $E_0 = (S^0, V^0, 0, 0)$ given by Eq. (18), and since there is only one infection variable, both Jacobians are scalars:

$$F = \left.\frac{\partial \mathcal{F}}{\partial I}\right|_{E_0} = \beta \left(\frac{S^0 + (1-\varepsilon)V^0}{N} \right), \tag{12}$$

$$V = \left.\frac{\partial \mathcal{V}}{\partial I}\right|_{E_0} = \gamma + \mu + \alpha. \tag{13}$$

The next-generation matrix is $K = FV^{-1}$, so

$$R_0 = \frac{F}{V} = \frac{\beta}{\gamma + \mu + \alpha} \cdot \frac{S^0 + (1-\varepsilon)V^0}{N}. \tag{14}$$

From Eq. (18), with $N = \Lambda/\mu$ at the DFE,

$$\frac{S^0}{N} = \frac{\mu + \sigma}{\mu + \sigma + \xi}, \qquad \frac{V^0}{N} = \frac{\xi}{\mu + \sigma + \xi} \quad \Longrightarrow \quad \frac{S^0 + (1-\varepsilon)V^0}{N} = \frac{(\mu + \sigma) + (1-\varepsilon)\xi}{\mu + \sigma + \xi}.$$

Substituting into Eq. (14) yields

$$\boxed{R_0 = \frac{\beta}{\gamma + \mu + \alpha} \cdot \frac{(\mu + \sigma) + (1-\varepsilon)\xi}{\mu + \sigma + \xi}}. \tag{15}$$

For measles, $\alpha = 0$, so $R_0 = \dfrac{\beta}{\gamma + \mu} \cdot \dfrac{(\mu + \sigma) + (1-\varepsilon)\xi}{\mu + \sigma + \xi}$, which serves as the primary threshold parameter for the stability and existence analysis below.

3.4. Equilibrium Points

3.4.1. Disease-Free Equilibrium (DFE)

At the DFE, $I = 0$ and $R = 0$; the R-equation is automatically satisfied, and the S, V dynamics reduce to

$$\Lambda - (\mu + \xi)S + \sigma V = 0, \tag{16}$$

$$\xi S - (\mu + \sigma)V = 0. \tag{17}$$

From Eq. (17), $V = \frac{\xi}{\mu+\sigma} S$. Substituting into Eq. (16) and simplifying the numerator, $(\mu+\xi)(\mu+\sigma) - \sigma\xi = \mu(\mu + \sigma + \xi)$, gives

$$S^0 = \frac{\Lambda(\mu + \sigma)}{\mu(\mu + \sigma + \xi)}, \qquad V^0 = \frac{\xi}{\mu + \sigma} S^0 = \frac{\xi \Lambda}{\mu(\mu + \sigma + \xi)}.$$

Thus the disease-free equilibrium is

$$E_0 = \left(S^0,\ V^0,\ 0,\ 0\right) = \left(\frac{\Lambda(\mu+\sigma)}{\mu(\mu+\sigma+\xi)},\ \frac{\xi\Lambda}{\mu(\mu+\sigma+\xi)},\ 0,\ 0\right). \tag{18}$$

Since $S^0 + V^0 = \Lambda/\mu$, consistent with the constant-population assumption, E_0 always lies in the feasible region Ω for all positive parameter values, so its existence requires no additional condition.

3.4.2. Endemic Equilibrium Point

Theorem 1 (Existence of the Endemic Point)**.** *The system Eq. (6)–Eq. (9) has a unique endemic equilibrium point $E^* = (S^*, V^*, I^*, R^*)$ with $I^* > 0$ in the interior of Ω if and only if $R_0 > 1$.*

Proof. Let $E^* = (S^*, V^*, I^*, R^*)$ with $I^* > 0$ satisfy the equilibrium equations of Eq. (6)–Eq. (9). Since $\alpha = 0$, the total population $N = \Lambda/\mu$ is constant, so $N^* = N$. Define the proportions

$$s^* = \frac{S^*}{N},\quad v^* = \frac{V^*}{N},\quad i^* = \frac{I^*}{N},\quad r^* = \frac{R^*}{N},\qquad s^* + v^* + i^* + r^* = 1.$$

From Eq. (9) at equilibrium, $R^* = \frac{\gamma}{\mu} I^*$, i.e. $r^* = \frac{\gamma}{\mu} i^*$. From Eq. (8) at equilibrium (dividing by NI^*, $I^* \neq 0$),

$$\beta s^* + (1-\varepsilon)\beta v^* = \gamma + \mu \equiv \delta. \tag{19}$$

From Eq. (7) at equilibrium (dividing by N),

$$v^* = \frac{\xi s^*}{(1-\varepsilon)\beta i^* + \mu + \sigma} =: \frac{\xi s^*}{D},\qquad D := (1-\varepsilon)\beta i^* + \mu + \sigma. \tag{20}$$

Substituting Eq. (20) into Eq. (19) and solving for s^*,

$$s^* = \frac{\delta}{\beta + \dfrac{(1-\varepsilon)\beta\xi}{D}} = \frac{\delta D}{\beta(D + (1-\varepsilon)\xi)}. \tag{21}$$

Using $s^* + v^* + i^* + r^* = 1$ together with Eq. (20) and $r^* = \frac{\gamma}{\mu} i^*$,

$$s^*\left(1 + \frac{\xi}{D}\right) = 1 - i^*\left(1 + \frac{\gamma}{\mu}\right) \iff s^* \cdot \frac{D+\xi}{D} = 1 - i^*\left(1 + \frac{\gamma}{\mu}\right). \tag{22}$$

Substituting Eq. (21) into Eq. (22) and simplifying the resulting ratio,

$$\frac{\delta D}{\beta(D + (1-\varepsilon)\xi)} \cdot \frac{D+\xi}{D} = \delta \cdot \frac{D+\xi}{\beta(D + (1-\varepsilon)\xi)} = 1 - i^*\left(1 + \frac{\gamma}{\mu}\right),$$

so that, after multiplying both sides by β and substituting back $D = (1-\varepsilon)\beta i^* + \mu + \sigma$,

$$\delta\left[(1-\varepsilon)\beta i^* + \mu + \sigma + \xi\right] = \beta\left[1 - i^*\left(1 + \frac{\gamma}{\mu}\right)\right]\left[(1-\varepsilon)\beta i^* + \mu + \sigma + (1-\varepsilon)\xi\right]. \tag{23}$$

Expanding Eq. (23) and collecting terms in i^* gives the quadratic

$$a_2 (i^*)^2 + a_1 i^* + a_0 = 0, \tag{24}$$

with

$$a_2 = (1-\varepsilon)\beta^2\left(1 + \frac{\gamma}{\mu}\right), \tag{25}$$

$$a_1 = \delta(1-\varepsilon)\beta - \beta^2(1-\varepsilon) + \beta\left(1+\frac{\gamma}{\mu}\right)(\mu+\sigma+(1-\varepsilon)\xi), \tag{26}$$

$$a_0 = \delta(\mu+\sigma+\xi) - \beta(\mu+\sigma+(1-\varepsilon)\xi). \tag{27}$$

By the definition of R_0 in Eq. (15) (with $\alpha = 0$), $\beta(\mu+\sigma+(1-\varepsilon)\xi) = \delta(\mu+\sigma+\xi)R_0$, so

$$a_0 = \delta(\mu+\sigma+\xi)(1-R_0). \tag{28}$$

Since $a_2 > 0$, the quadratic Eq. (24) has exactly one positive root if and only if $a_0 < 0$, i.e. $R_0 > 1$, given by

$$i^* = \frac{-a_1 + \sqrt{a_1^2 - 4a_2a_0}}{2a_2}, \qquad I^* = Ni^* = \frac{\Lambda}{\mu}i^*, \qquad R^* = \frac{\gamma}{\mu}I^*. \tag{29}$$

The remaining components follow directly from I^*. From Eq. (7) at equilibrium,

$$V^* = \frac{\xi S^*}{(1-\varepsilon)\beta\frac{I^*}{N} + \mu + \sigma}. \tag{30}$$

Substituting Eq. (30) into Eq. (6) at equilibrium and solving for S^*,

$$S^* = \frac{\Lambda}{\beta\frac{I^*}{N} + \mu + \xi - \dfrac{\sigma\xi}{(1-\varepsilon)\beta\frac{I^*}{N} + \mu + \sigma}}. \tag{31}$$

Positivity of S^* follows since

$$\frac{\sigma\xi}{(1-\varepsilon)\beta\frac{I^*}{N} + \mu + \sigma} < \frac{\sigma\xi}{\sigma} = \xi \implies \beta\frac{I^*}{N} + \mu + \xi - \frac{\sigma\xi}{(1-\varepsilon)\beta\frac{I^*}{N} + \mu + \sigma} > \beta\frac{I^*}{N} + \mu > 0,$$

and positivity of V^*, R^* then follows from Eq. (30) and Eq. (29).
Equivalently, i^* is the positive root of

$$\frac{\beta\mu[(1-\varepsilon)\beta i + \mu + \sigma + (1-\varepsilon)\xi]}{(\beta i + \mu + \xi)((1-\varepsilon)\beta i + \mu + \sigma) - \sigma\xi} = \mu + \gamma, \tag{32}$$

which, by Eq. (28), has exactly one positive solution precisely when $R_0 > 1$. Hence, for $R_0 > 1$ all components of $E^* = (S^*, V^*, I^*, R^*)$ as given by Eq. (29)–Eq. (31) are positive and lie in the interior of Ω. □

3.5. Stability Analysis

3.5.1. Stability Analysis of the Disease-Free Equilibrium

The stability of the disease-free equilibrium $E_0 = (S^0, V^0, 0, 0)$ is analyzed locally via linearization and globally via Lyapunov functions.

Theorem 2 (Local Stability of DFE). *The disease-free equilibrium point E_0 is locally asymptotically stable if $R_0 < 1$.*

Proof. The Jacobian matrix of the system Eq. (6)–Eq. (9) evaluated at E_0 is given by

$$J(E_0) = \begin{pmatrix} -(\mu+\xi) & \sigma & -\beta\dfrac{S^0}{N} & 0 \\ \xi & -(\mu+\sigma) & -(1-\varepsilon)\beta\dfrac{V^0}{N} & 0 \\ 0 & 0 & \beta\dfrac{S^0}{N} + (1-\varepsilon)\beta\dfrac{V^0}{N} - (\gamma+\mu+\alpha) & 0 \\ 0 & 0 & \gamma & -\mu \end{pmatrix}. \tag{33}$$

Since the matrix has a block-triangular structure, the eigenvalues are directly obtained from the diagonal elements:

$$\lambda_1 = -\mu, \quad \lambda_2 = -(\mu+\xi+\sigma), \quad \lambda_4 = -\mu,$$

all of which are negative, and

$$\lambda_3 = \beta\frac{S^0}{N} + (1-\varepsilon)\beta\frac{V^0}{N} - (\gamma+\mu+\alpha).$$

Using the definition of R_0 in Eq. (15) along with the ratios $S^0/N = (\mu+\sigma)/(\mu+\sigma+\xi)$ and $V^0/N = \xi/(\mu+\sigma+\xi)$, we obtain

$$\lambda_3 = (\gamma+\mu+\alpha)(R_0 - 1).$$

If $R_0 < 1$, then $\lambda_3 < 0$, so all eigenvalues are negative. This guarantees the local asymptotic stability of E_0. □

Lemma 1 (Comparison Bound for (S, V))**.** *For any solution of Eq. (6)–Eq. (9) in* Ω*,*

$$\limsup_{t\to\infty} S(t) \le S^0, \qquad \limsup_{t\to\infty} V(t) \le V^0. \tag{34}$$

Proof. Since $I \ge 0$,

$$\dot{S} \le \Lambda - (\mu+\xi)S + \sigma V, \qquad \dot{V} \le \xi S - (\mu+\sigma)V. \tag{35}$$

Let $(\bar{S}, \bar{V})$ solve the corresponding equality system, with $\bar{S}(0) = S(0), \bar{V}(0) = V(0)$,

$$\dot{\bar{S}} = \Lambda - (\mu+\xi)\bar{S} + \sigma\bar{V}, \qquad \dot{\bar{V}} = \xi\bar{S} - (\mu+\sigma)\bar{V}, \tag{36}$$

with coefficient matrix

$$A = \begin{pmatrix} -(\mu+\xi) & \sigma \\ \xi & -(\mu+\sigma) \end{pmatrix},$$

$$\det(A - \lambda I) = (\lambda+\mu)(\lambda+\mu+\xi+\sigma) = 0 \;\Rightarrow\; \lambda_{1,2} = -\mu, -(\mu+\xi+\sigma) < 0. \tag{37}$$

A has non-negative off-diagonal entries (cooperative), so by Eq. (35) and the comparison principle, $S \le \bar{S}$, $V \le \bar{V}$ for all $t \ge 0$. As $\lambda_{1,2} < 0$, $(\bar{S}, \bar{V}) \to (S^0, V^0)$, giving the result. □

Theorem 3 (Global Stability of the DFE)**.** *The disease-free equilibrium* $E_0 = (S^0, V^0, 0, 0)$ *is globally asymptotically stable on* Ω *if* $R_0 < 1$*.*

Proof. Define $\mathcal{L}(t) = I(t)$. Clearly $\mathcal{L} \geq 0$ for all t, and $\mathcal{L} = 0$ iff $I = 0$, so $\mathcal{L}$ is positive definite relative to $\{I = 0\}$. Along solutions of Eq. (8),

$$\dot{\mathcal{L}} = \dot{I} = \Big(\beta\frac{S}{N} + (1-\varepsilon)\beta\frac{V}{N}\Big)I - \delta I, \qquad \delta := \gamma + \mu + \alpha. \tag{38}$$

1: Eventual sign of $\dot{\mathcal{L}}$. Since $R_0 < 1$, i.e. $\beta S^0 + (1-\varepsilon)\beta V^0 < N\delta$, fix

$$0 < \eta_0 < \frac{N\delta - \beta S^0 - (1-\varepsilon)\beta V^0}{\beta + (1-\varepsilon)\beta}, \tag{39}$$

so that, by construction,

$$\beta(S^0 + \eta_0) + (1-\varepsilon)\beta(V^0 + \eta_0) < N\delta. \tag{40}$$

By Lemma 1, $\limsup_{t\to\infty} S(t) \leq S^0$. By definition, $\limsup_{t\to\infty} S(t) = \lim_{T\to\infty} \sup_{t\geq T} S(t)$, and $T \mapsto \sup_{t\geq T} S(t)$ is non-increasing in T; since this limit is $\leq S^0 < S^0 + \eta_0$, there exists T_1 such that

$$\sup_{t\geq T_1} S(t) < S^0 + \eta_0, \quad \text{hence} \quad S(t) < S^0 + \eta_0 \ \ \forall\, t \geq T_1. \tag{41}$$

Identically, from $\limsup_{t\to\infty} V(t) \leq V^0$, there exists T_2 with $V(t) < V^0 + \eta_0$ for all $t \geq T_2$. Define

$$T_{\eta_0} := \max(T_1, T_2), \tag{42}$$

so that both bounds hold simultaneously for $t \geq T_{\eta_0}$. Substituting $S(t) < S^0 + \eta_0$, $V(t) < V^0 + \eta_0$ into Eq. (38) and using Eq. (40),

$$\dot{\mathcal{L}}(t) < \Big[\frac{\beta(S^0 + \eta_0) + (1-\varepsilon)\beta(V^0 + \eta_0)}{N} - \delta\Big] I(t) =: -c\, I(t), \qquad c > 0, \qquad t \geq T_{\eta_0}. \tag{43}$$

Since $I(t) \geq 0$ for all t, Eq. (43) gives $\dot{\mathcal{L}}(t) \leq 0$ for $t \geq T_{\eta_0}$, with equality only if $I(t) = 0$.

2: Existence of the limit $\mathcal{L}_\infty$. By Eq. (43), $\mathcal{L}$ is non-increasing on $[T_{\eta_0}, \infty)$; also $\mathcal{L}(t) = I(t) \geq 0$ for all t, so $\mathcal{L}$ is bounded below by 0 on this interval. By the Monotone Convergence Theorem for real-valued functions, the limit

$$\mathcal{L}_\infty := \lim_{t\to\infty} \mathcal{L}(t) = \inf_{t\geq T_{\eta_0}} \mathcal{L}(t) \tag{44}$$

exists and satisfies $\mathcal{L}_\infty \geq 0$.

3: Omega-limit set. Because Ω is compact and positively invariant, the omega-limit set ω of the solution is non-empty, compact, and invariant under the flow of Eq. (6)–Eq. (9). By continuity of $\mathcal{L}$ and Eq. (44), $\mathcal{L} \equiv \mathcal{L}_\infty$ on ω. For any point in ω, invariance means the trajectory through it remains in ω for all t, along which $\mathcal{L}$ is constant, so $\dot{\mathcal{L}} \equiv 0$; by Eq. (43), this forces $I \equiv 0$ along that trajectory. Hence $\omega \subset \{I = 0\}$.

4: Reduction on $\{I = 0\}$. On $\{I = 0\}$, $\dot{R} = -\mu R$, so $R \equiv 0$ on any bounded invariant set contained in $\{I = 0\}$ (a nonzero R would decay strictly, contradicting invariance), and the system restricted to ω reduces exactly to the linear system Eq. (36) for (S, V), with coefficient matrix A from Eq. (37) (Lemma 1) having eigenvalues $-\mu$ and $-(\mu + \xi + \sigma)$, both strictly negative. For a linear system with all eigenvalues in the open left half-plane, the only trajectory that remains bounded for all t is the equilibrium itself, since every other

trajectory grows unboundedly under the reversed (backward-time) flow. As ω is compact, invariant, and contained in $\{I = 0\}$, this forces

$$\omega = \{(S^0, V^0, 0, 0)\} = \{E_0\}. \tag{45}$$

Since $\omega = \{E_0\}$ is a single point, every solution starting in Ω converges to it, that is, $(S(t), V(t), I(t), R(t)) \to E_0$ as $t \to \infty$. As $\mathcal{L}$ is positive definite relative to $\{I = 0\}$ and the argument above holds for every initial condition in Ω, E_0 is globally asymptotically stable on Ω whenever $R_0 < 1$. □

3.5.2. Stability Analysis of the Endemic Point

Theorem 4 (Local Stability of the Endemic Point)**.** *If $R_0 > 1$, then the endemic equilibrium point E^* is locally asymptotically stable.*

Proof. To analyze the local stability of the endemic equilibrium point E^*, we linearize the system around that point. Since the total population N is constant, the system can be reduced to the first three equations in terms of the variables S, V, I. Using the ratios $s = S/N$, $v = V/N$, $i = I/N$ and recalling that at E^* we have $\beta s^* + (1-\varepsilon)\beta v^* = \gamma + \mu$ (Equation Eq. (32)), the Jacobian matrix evaluated at E^* is

$$J(E^*) = \begin{pmatrix} -\beta i^* - (\mu + \xi) & \sigma & -\beta s^* \\ \xi & -(1-\varepsilon)\beta i^* - (\mu + \sigma) & -(1-\varepsilon)\beta v^* \\ \beta i^* & (1-\varepsilon)\beta i^* & 0 \end{pmatrix}. \tag{46}$$

The characteristic equation $\det(\lambda I - J(E^*)) = 0$ yields a cubic polynomial

$$\lambda^3 + A_2\lambda^2 + A_1\lambda + A_0 = 0, \tag{47}$$

with coefficients

$$A_2 = \beta i^*(2-\varepsilon) + 2\mu + \xi + \sigma,$$
$$A_1 = \beta^2 i^* s^* + (1-\varepsilon)^2\beta^2 i^* v^* + (\beta i^* + \mu + \xi)\big((1-\varepsilon)\beta i^* + \mu + \sigma\big) - \sigma\xi,$$
$$A_0 = \beta i^*\Big[\beta s^*\big((1-\varepsilon)\beta i^* + \mu + \sigma + (1-\varepsilon)\xi\big) + (1-\varepsilon)\beta v^*\big(\sigma + (1-\varepsilon)(\beta i^* + \mu + \xi)\big)\Big].$$

The Routh–Hurwitz criterion for a cubic polynomial requires that all coefficients A_2, A_1, A_0 be positive and that $A_1A_2 - A_0 > 0$. Clearly, $A_2 > 0$ since all parameters are positive and $i^* > 0$. For A_1, the last term can be written as

$$(\beta i^* + \mu + \xi)((1-\varepsilon)\beta i^* + \mu + \sigma) - \sigma\xi > \mu(\mu + \xi + \sigma) > 0,$$

so $A_1 > 0$. The positivity of A_0 follows directly from $i^* > 0$ and the fact that all terms inside the square brackets are positive. Furthermore, $A_1A_2 - A_0$ can be factored as

$$A_1A_2 - A_0 = i^*\Big[\beta^2 i^*\big((1-\varepsilon)^2 v^* + s^*\big) + \beta(\mu + \sigma + \xi)\big((1-\varepsilon)\beta i^* + \mu + \sigma + \xi\big) + \mu(\mu + \sigma)\big(2\mu + \xi + \sigma + \beta i^*(2-\varepsilon)\big)\Big].$$

All terms inside the square brackets are sums of positive terms, so $A_1A_2 - A_0 > 0$ if and only if $i^* > 0$.

For completeness, the Routh table for the characteristic polynomial above is

λ^3	1	A_1	0
λ^2	A_2	A_0	0
λ^1	$\dfrac{A_2A_1 - A_0}{A_2}$	0	0
λ^0	A_0	0	0

The condition for local asymptotic stability is that all entries in the first column are positive, namely $1 > 0$, $A_2 > 0$, $(A_2A_1 - A_0)/A_2 > 0$, and $A_0 > 0$. Since $A_2 > 0$, the third condition is equivalent to $A_1A_2 - A_0 > 0$. Thus, the four Routh–Hurwitz conditions are satisfied if and only if $A_2 > 0$, $A_0 > 0$, and $A_1A_2 > A_0$, all of which hold exactly when $i^* > 0$. From the existence condition for the endemic equilibrium, $i^* > 0$ is equivalent to $R_0 > 1$. Therefore, E^* is locally asymptotically stable. □

Theorem 5 (Global Stability of the Endemic Equilibrium). *Suppose $R_0 > 1$, so the endemic equilibrium $E^* = (s^*, v^*, i^*)$ exists (Theorem 3), and suppose the parameters satisfy*

$$M^2 \le 4\mu(M + \sigma), \qquad M := (1 - \varepsilon)\beta i^* + \mu. \tag{48}$$

Then E^* is globally asymptotically stable in $\mathrm{int}(\Omega)$.

Proof. Let $x = s/s^*$, $y = v/v^*$, $z = i/i^*$ and define

$$L(s, v, i) = \left(s - s^* - s^* \ln \tfrac{s}{s^*}\right) + \left(v - v^* - v^* \ln \tfrac{v}{v^*}\right) + \left(i - i^* - i^* \ln \tfrac{i}{i^*}\right). \tag{49}$$

Since $\eta - 1 - \ln \eta \ge 0$ for $\eta > 0$ with equality iff $\eta = 1$, L is positive definite on $\mathrm{int}(\Omega)$ and vanishes only at E^*.

(Reduction). Using the equilibrium relations

$$\mu = \beta s^* i^* + (\mu + \xi)s^* - \sigma v^*, \tag{50}$$
$$\xi s^* = (1 - \varepsilon)\beta v^* i^* + (\mu + \sigma)v^*, \tag{51}$$
$$\gamma + \mu = \beta s^* + (1 - \varepsilon)\beta v^*. \tag{52}$$

system Eq. (6)–Eq. (8) becomes, in terms of x, y, z,

$$\dot{s} = \beta s^* i^* x(1 - z) + \mu(1 - x) + \sigma v^*(y - x), \tag{53}$$
$$\dot{v} = (1 - \varepsilon)\beta v^* i^* y(1 - z) + \xi s^*(x - y), \tag{54}$$
$$\dot{i} = i^* z[\beta s^* x + (1 - \varepsilon)\beta v^* y - (\gamma + \mu)]. \tag{55}$$

Then, invoking the chain rule for the total derivative of L along trajectories of Eq. (6)–Eq. (8),

$$\dot{L} = \left(1 - \frac{1}{x}\right)\dot{s} + \left(1 - \frac{1}{y}\right)\dot{v} + \left(1 - \frac{1}{z}\right)\dot{i}. \tag{56}$$

Substituting the reduced dynamics Eq. (53)–Eq. (55) and using the elementary identity $(1 - 1/\eta)\,\eta = \eta - 1$ term by term,

$$\left(1 - \frac{1}{x}\right)\dot{s} = \beta s^* i^*(1 - z)(x - 1) - \mu\frac{(x - 1)^2}{x} + \sigma v^*\frac{(y - x)(x - 1)}{x} \tag{57}$$

$$\left(1 - \frac{1}{y}\right)\dot{v} = (1 - \varepsilon)\beta v^* i^*(1 - z)(y - 1) + \xi s^*\frac{(x - y)(y - 1)}{y}, \tag{58}$$

$$\left(1 - \frac{1}{z}\right)\dot{i} = i^*(z - 1)[\beta s^* x + (1 - \varepsilon)\beta v^* y - (\gamma + \mu)]. \tag{59}$$

Summing Eq. (57)–Eq. (59) and grouping the terms carrying the factor $(1-z)$ (equivalently $(z-1)$) separately from those that do not,

$$\dot{L} = T_z + R, \tag{60}$$

where

$$T_z = \beta s^* i^*(x-1)(1-z)+(1-\varepsilon)\beta v^* i^*(y-1)(1-z)+i^*(z-1)\big[\beta s^* x+(1-\varepsilon)\beta v^* y-(\gamma+\mu)\big] \tag{61}$$

and

$$R = -\mu\frac{(x-1)^2}{x} + \sigma v^*\frac{(y-x)(x-1)}{x} + \xi s^*\frac{(x-y)(y-1)}{y}. \tag{62}$$

1: $T_z \equiv 0$. Factor $i^*(1-z)$ out of the first two terms of Eq. (61) and write $(z-1) = -(1-z)$ in the third, so that

$$T_z = i^*(1-z)\Big\{\big[\beta s^*(x-1) + (1-\varepsilon)\beta v^*(y-1)\big] - \big[\beta s^* x + (1-\varepsilon)\beta v^* y - (\gamma+\mu)\big]\Big\}. \tag{63}$$

Expanding the bracketed difference,

$$\begin{aligned}
&\big[\beta s^* x - \beta s^* + (1-\varepsilon)\beta v^* y - (1-\varepsilon)\beta v^*\big] - \big[\beta s^* x + (1-\varepsilon)\beta v^* y - (\gamma+\mu)\big] \\
&= \beta s^* x - \beta s^* x + (1-\varepsilon)\beta v^* y - (1-\varepsilon)\beta v^* y - \beta s^* - (1-\varepsilon)\beta v^* + (\gamma+\mu) \\
&= (\gamma+\mu) - \big[\beta s^* + (1-\varepsilon)\beta v^*\big].
\end{aligned} \tag{64}$$

Since (s^*, v^*, i^*) is by construction the endemic equilibrium of Eq. (6)–Eq. (8), it satisfies the force-of-infection balance relation Eq. (52), $\gamma+\mu = \beta s^* + (1-\varepsilon)\beta v^*$; substituting this identity into Eq. (64) collapses the bracket exactly to zero, and hence, from Eq. (63),

$$T_z = i^*(1-z)\cdot 0 = 0 \qquad \text{for all } x, y, z. \tag{65}$$

Consequently, by Eq. (60), $\dot{L}$ reduces exactly to R and is independent of z.

2: reduction of R to $N(x,y)/(xy)$. Multiplying Eq. (62) through by xy,

$$xy\,R = -\mu y(x-1)^2 + \sigma v^* y(y-x)(x-1) + \xi s^* x(x-y)(y-1). \tag{66}$$

Writing $(y-x) = -(x-y)$ in the second term of Eq. (66),

$$xy\,R = -\mu y(x-1)^2 - \sigma v^* y(x-y)(x-1) + \xi s^* x(x-y)(y-1). \tag{67}$$

From the equilibrium relation Eq. (**??**), $\xi s^* = (1-\varepsilon)\beta v^* i^* + (\mu+\sigma)v^*$, which we write as $\xi s^* = K + \sigma v^*$ with $K := (1-\varepsilon)\beta v^* i^* + \mu v^* > 0$. Substituting into the last term of Eq. (67),

$$\xi s^* x(x-y)(y-1) = Kx(x-y)(y-1) + \sigma v^* x(x-y)(y-1). \tag{68}$$

Collecting the two terms in Eq. (67)–Eq. (68) that carry the factor σv^*,

$$\begin{aligned}
-\sigma v^* y(x-y)(x-1) + \sigma v^* x(x-y)(y-1) &= \sigma v^*(x-y)\big[x(y-1) - y(x-1)\big] \\
&= \sigma v^*(x-y)\big[xy - x - xy + y\big] \\
&= \sigma v^*(x-y)(y-x) \\
&= -\sigma v^*(x-y)^2.
\end{aligned} \tag{69}$$

Substituting Eq. (69) back into Eq. (67)–Eq. (68) gives

$$xy\,R = Kx(x-y)(y-1) - \mu y(x-1)^2 - \sigma v^*(x-y)^2 =: N(x,y), \tag{70}$$

so that, combining Eq. (60), Eq. (65), and Eq. (70),

$$\dot{L} = \frac{N(x,y)}{xy}. \tag{71}$$

3: sign of $N(x,y)$. Regard N in Eq. (70) as a quadratic in x, $N(x,y) = A(y)x^2 + B(y)x + C(y)$, with

$$A(y) = K(y-1) - \mu y - \sigma v^*, \qquad C(y) = N(0,y) = -y(\mu + \sigma v^* y) < 0 \ \ \forall\, y > 0. \tag{72}$$

Case (i): $y \in (0,1]$. Since $K > 0$ and $y - 1 \le 0$, $K(y-1) \le 0$; combined with $-\mu y - \sigma v^* < 0$, this gives $A(y) \le -\mu y - \sigma v^* < 0$. With $A(y) < 0$ (downward-opening parabola in x) and $C(y) < 0$, and noting that $N(1,y) = -(K + \sigma v^*)(y-1)^2 \le 0$ with equality only at $y = 1$, the parabola $N(\cdot, y)$ is non-positive on $x > 0$, vanishing only at the stationary point $(x,y) = (1,1)$.
Case (ii): $y \in (1, 1/v^*)$. Here $y - 1 > 0$. Evaluating $A(y)$ at the upper endpoint $y_{\max} = 1/v^*$ and substituting Eq. (51) reduces the requirement $A(y_{\max}) < 0$ to

$$w^2 - Mw + \mu(M + \sigma) > 0, \qquad w := \xi s^*, \quad M := (1-\varepsilon)\beta i^* + \mu. \tag{73}$$

This holds for every $w > 0$ precisely when the discriminant of Eq. (73) is non-positive, i.e. under condition Eq. (48), $M^2 \le 4\mu(M + \sigma)$. Since $A(y)$ is affine in y and is negative at both endpoints $y = 1$ and $y = y_{\max}$, it follows that $A(y) < 0$ throughout $(1, y_{\max})$ as well. Hence $N(x,y) \le 0$ on the full domain $x, y > 0$, with equality only at $(1,1)$, and therefore, by Eq. (71), $\dot{L} \le 0$ on $\mathrm{int}(\Omega)$, vanishing only at $x = y = 1$.
Since $L \ge 0$ and $\dot{L} \le 0$ on $\mathrm{int}(\Omega)$ (Steps 1–2), $L(t)$ is non-increasing and bounded below, so $L(t) \to L_\infty \ge 0$ as $t \to \infty$ for any solution starting in $\mathrm{int}(\Omega)$. Because $\bar{\Omega}$ is compact and positively invariant, the omega-limit set ω of any such solution is non-empty, compact, and invariant under the flow of Eq. (6)–Eq. (9); by continuity of L and monotone convergence of $L(t)$, $L \equiv L_\infty$ is constant on ω.
Let $(\bar{s}, \bar{v}, \bar{\imath}) \in \omega$. Since ω is invariant, the solution through $(\bar{s}, \bar{v}, \bar{\imath})$ remains in ω for all t, on which $L \equiv L_\infty$ is constant, so $\dot{L} \equiv 0$ along this solution. By Step 2, this forces $\bar{s} = s^*$, $\bar{v} = v^*$.
To see that $\bar{\imath} = i^*$ is also forced, evaluate $\dot{s}$ and $\dot{v}$ directly at $s = s^*, v = v^*$ (with i left free). Using Eq. (53)–Eq. (54) together with (39) and (40),

$$\dot{s}\big|_{s=s^*, v=v^*} = \beta s^*(i^* - i), \qquad \dot{v}\big|_{s=s^*, v=v^*} = (1-\varepsilon)\beta v^*(i^* - i). \tag{74}$$

Since ω is invariant, $s \equiv s^*$ and $v \equiv v^*$ must persist for all t along the solution through $(\bar{s}, \bar{v}, \bar{\imath})$, which requires $\dot{s} = \dot{v} = 0$ identically; by Eq. (74), since $\beta s^* > 0$ and $(1-\varepsilon)\beta v^* > 0$, this holds only if $i \equiv i^*$. Hence $\bar{\imath} = i^*$, so $\omega = \{E^*\}$.
Since ω is a single point, every solution converges to it: $(s(t), v(t), i(t)) \to E^*$ as $t \to \infty$ for all initial conditions in $\mathrm{int}(\Omega)$. As L is positive definite, E^* is therefore globally asymptotically stable whenever $R_0 > 1$. □

Corollary 1. *Condition Eq. (48) is satisfied by the parameters estimated in Section 3 ($\beta = 0.6422, \gamma = 0.3485, \mu = 2.75 \times 10^{-4}, \xi = 0.0224, \sigma = 0.0072$) with $\varepsilon = 0.5$ — the only scenario in this study with $R_0 > 1$ — since $M \approx 3.08 \times 10^{-4}$ gives $M^2 - 4\mu(M + \sigma) \approx -8.16 \times 10^{-6} < 0$. Theorem 5 therefore applies rigorously to the endemic regime simulated in Section 4.3.*

Remark 1. This corrects the Lyapunov function originally proposed, which included an additional weighting factor $\sigma v^*/(\xi s^*)$ on the V-logarithmic term; symbolic and numerical verification shows this weighting is invalid, and the unweighted form Eq. (49) is the correct choice, yielding the exact simplification in Step 1 of the proof whereby dL/dt depends only

on s and v. Theorem 5 holds under the sufficient condition Eq. (48), which is satisfied with considerable margin by the parameters estimated from the Sidoarjo data (Corollary 1); establishing it for a broader parameter class is left for future work. The convergence argument in Step 3 is derived explicitly via the omega-limit set of the flow — see Eq. (74) — so that the reduction of the largest invariant subset of $\{\dot{L} = 0\}$ to $\{E^*\}$ is fully transparent rather than invoked as a black-box result.

4. Numerical Simulation

To validate the stability analysis results, a numerical simulation was conducted using weekly measles case data from Sidoarjo City throughout 2023. The data were obtained from the Sidoarjo City Health Office and Badan Pusat Statistik (BPS) [22, 23].

4.1. Parameter Estimation

Parameter estimation was performed using four methods: *Ensemble Kalman Filter* (EKF), *Least Squares* (LS), *Maximum Likelihood Estimation* (MLE), and *Particle Swarm Optimization* (PSO). All three error metrics (MAPE, RMSE, MAE) are computed against weekly incidence, ensuring internal consistency across methods. Based on the evaluation of performance metrics, PSO provided the best results with the lowest MAPE of 10.82%. Table 3 presents a brief comparison, and therefore the PSO parameters were selected as the reference parameters for all simulations.

Table 3: Comparison of Estimation Method Performance (Weekly Incidence).

Method	MAPE (%)	RMSE	MAE
EKF	119.71	5522.71	4235.22
LS	64.66	2961.64	2353.54
MLE	30.48	956.82	740.97
PSO	**10.82**	**202.64**	**189.55**

The parameter estimates obtained using PSO are $\beta = 0.6422$, $\gamma = 0.3485$, $\xi = 0.0224$, and $\sigma = 0.0072$; the biological plausibility of the estimated waning rate σ is discussed in Section 5. Figure 2 shows that the simulation using PSO parameters produces the cumulative case curve that most closely matches the observed data for Sidoarjo City, East Java, Indonesia.

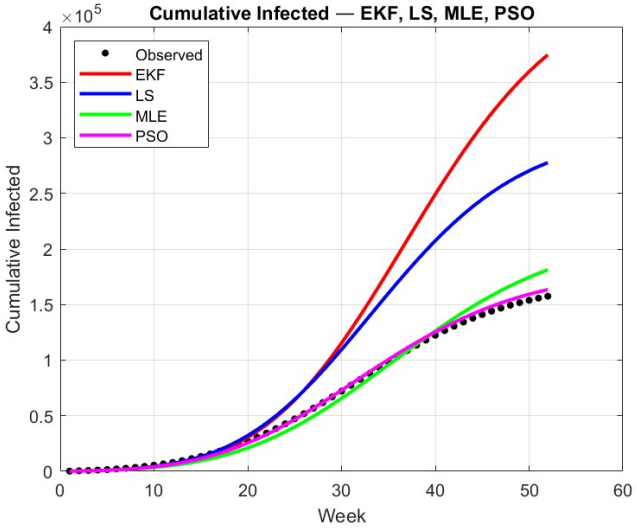

Fig. 2: Comparison of cumulative infection cases in Sidoarjo: observed vs. simulated using various methods.

4.2. Validation of Stability Analysis Results

Using the PSO parameters, the basic reproduction number is calculated using Equation Eq. (15):

$$R_0 = \frac{0.6422}{0.3485 + 0.000275} \cdot \frac{(0.000275 + 0.0072) + (0.15)(0.0224)}{0.000275 + 0.0072 + 0.0224} \approx 0.668. \quad (75)$$

The value $R_0 = 0.668 < 1$ indicates that, consistent with the analytical results, the system is in the disease-free regime. The disease-free equilibrium point (E_0) is globally asymptotically stable, meaning the disease will not persist in the population in the long run.

A simulation of the system dynamics with PSO parameters is shown in Figure 4. It can be seen that the number of infected individuals (I) decreases progressively toward zero, confirming convergence toward the disease-free point.

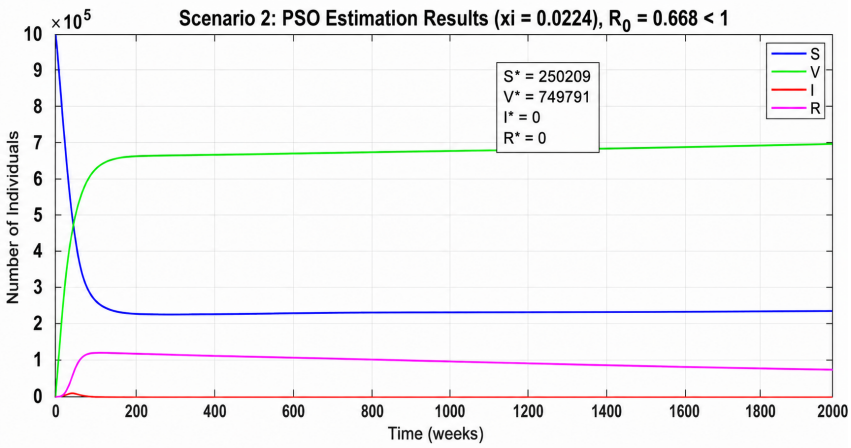

Fig. 3: Dynamics of the SVIR model with PSO-estimated parameters ($R_0 = 0.668$). The system converges to the disease-free point.

4.3. Sensitivity Analysis of Vaccine Effectiveness (ε)

Before performing a numerical sensitivity analysis, the sensitivity index of each model parameter with respect to R_0 is first examined. The sensitivity index (*normalized sensitivity index*) of a parameter p with respect to R_0 is defined as:

$$\Upsilon_p^{R_0} = \frac{\partial R_0}{\partial p} \cdot \frac{p}{R_0}, \quad (76)$$

which measures the percentage change in R_0 resulting from a one-percent change in the parameter p. A positive sensitivity index value indicates that an increase in the parameter p will increase R_0, while a negative value indicates an inverse relationship. For comparison purposes and to determine the most influential parameter, the absolute value $\left|\Upsilon_p^{R_0}\right|$ is used, since what is being examined is the magnitude of the effect, not merely the direction of the change.

The results of the sensitivity index calculations for all model parameters are presented in Figure 4.

Based on Figure 4, the vaccine effectiveness parameter (ε) has a sensitivity index value of $\Upsilon_\varepsilon^{R_0} = -5{,}9$, which is the largest absolute value among all model parameters. The negative sign of this index confirms that the relationship between ε and R_0 is inversely proportional: a 1% increase in vaccine effectiveness will result in a 5.9% decrease in R_0, assuming all other parameters remain constant. The magnitude of the absolute value of this sensitivity index indicates that ε is the most dominant parameter in determining the value of R_0, so even a small change in vaccine effectiveness will have a significant impact on the overall dynamics of disease spread. Therefore, the numerical sensitivity analysis focuses on the parameter ε to examine in greater depth its practical implications for disease control.

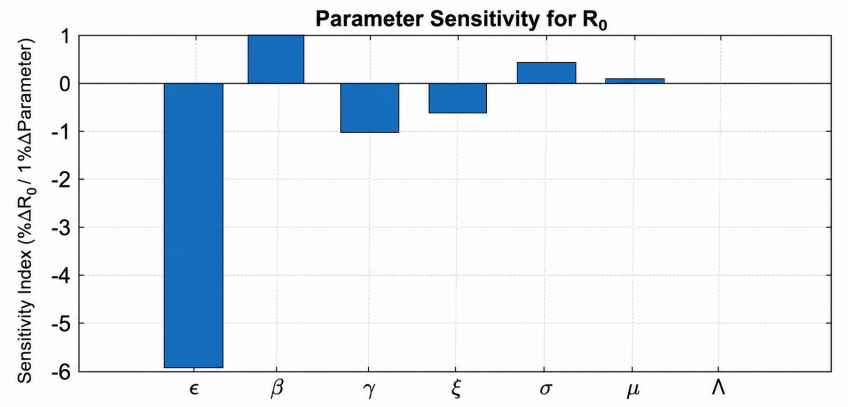

Fig. 4: Sensitivity index of SVIR model parameters with respect to R_0.

To quantify this effect, three ε value scenarios were examined: namely $\varepsilon = 0.5$ (low effectiveness), $\varepsilon = 0.75$ (moderate effectiveness), and $\varepsilon = 0.85$ (PSO/existing estimate), while all other parameters are maintained according to the PSO estimates.

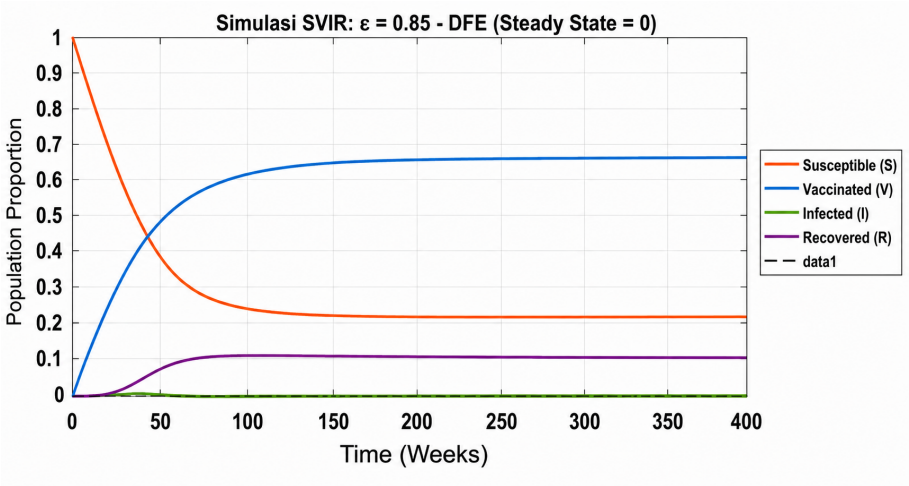

Fig. 5: Dynamics of the SVIR model with $\varepsilon = 0.85$.

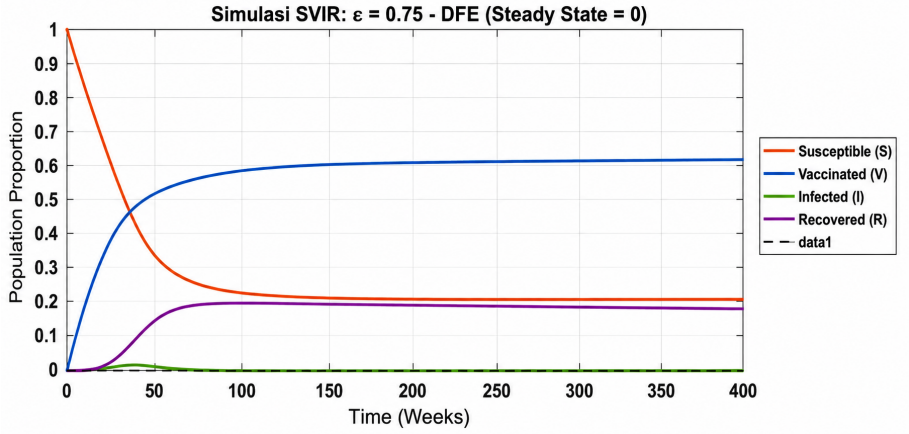

Fig. 6: Dynamics of the SVIR model with $\varepsilon = 0.75$.

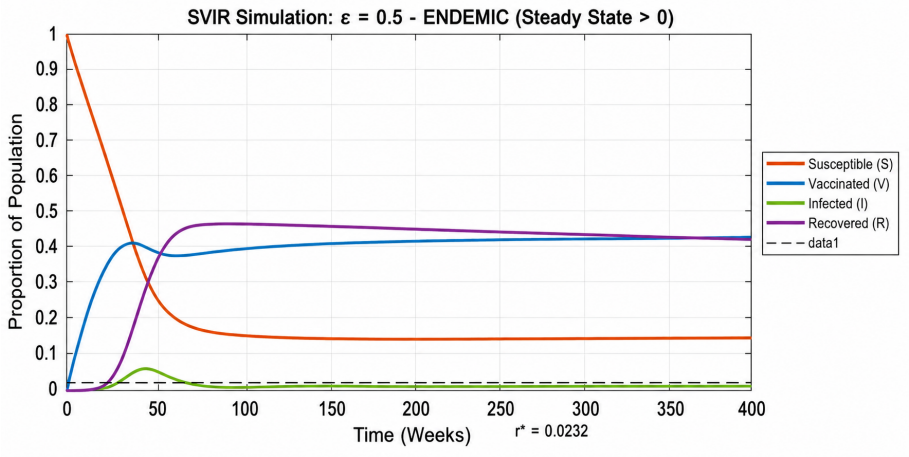

Fig. 7: Dynamics of the SVIR model with $\varepsilon = 0.5$.

The results in Figures 7–5 show that vaccine effectiveness has a significant and monotonic effect on the value of R_0 and the dynamic behavior of all compartments in the SVIR model. The following provides a systematic interpretation for each scenario.

Scenario 1: $\varepsilon = 0.85$ **(Existing Value/PSO).** This scenario represents the existing conditions obtained from parameter estimation using the PSO method, with $R_0 = 0.668$. This value is the smallest among the three scenarios, indicating that under the existing conditions, the system is furthest from the critical threshold $R_0 = 1$. Consequently, the decline in the number of infected individuals occurs at the fastest rate, as shown in Figure 5, where the $I(t)$ curve decreases more steeply and reaches a value close to zero within a shorter timeframe compared to the other two scenarios. This condition describes a situation where the vaccination program is running effectively and the population is in a state that is safe from the risk of a resurgence in the short term.

Scenario 2: $\varepsilon = 0{,}75$ **(Moderate Effectiveness).** In the moderate effectiveness scenario, $R_0 = 0.782 < 1$ is obtained, indicating that the disease-free equilibrium point E_0 is locally asymptotically stable. This means the disease will gradually subside, and the number of infected individuals will decrease exponentially toward zero over time. This can be observed in Figure 6, where the curve $I(t)$ shows a consistent downward trend. However, the rate of decline in this scenario is slower compared to the existing condition scenario (Scenario 1), due to a larger value of R_0 that is closer to the critical threshold $R_0 = 1$. The safety margin $(1 - R_0)$ shrinks from 0.332 at $\varepsilon = 0.85$ to 0.218 at $\varepsilon = 0.75$ — a 34% reduction in buffer capacity; despite R_0 remaining below the epidemic threshold. This condition indicates that the system is in a relatively more vulnerable state: a small disturbance in other parameters, such as an increase in the rate of contact between individuals or a decrease in vaccination coverage, has the potential to push R_0 beyond the value of one and reverse the previously controlled condition into an endemic one. This demonstrates that even a modest decrease in vaccine effectiveness from the current level ($\varepsilon = 0.85$ to $\varepsilon = 0.75$) significantly erodes the safety margin and shifts the system into a precariously vulnerable state, well before the critical threshold is breached.

Scenario 3: $\varepsilon = 0.5$ **(Low Effectiveness).** In this scenario, $R_0 = 1.151 > 1$, which mathematically implies that the disease-free equilibrium point E_0 is unstable. Based on stability theory, when $R_0 > 1$, each infected individual will, on average, transmit the disease to more than one other individual during the infection period, so the disease cannot be controlled and will become endemic in the population. This condition is reflected in Figure 7, where the number of infected individuals $I(t)$ does not tend toward zero but rather stabilizes at a positive value in the long

run. Vaccination with an effectiveness of 50% has proven insufficient to establish herd immunity in the population, so additional interventions beyond vaccination remain absolutely necessary.

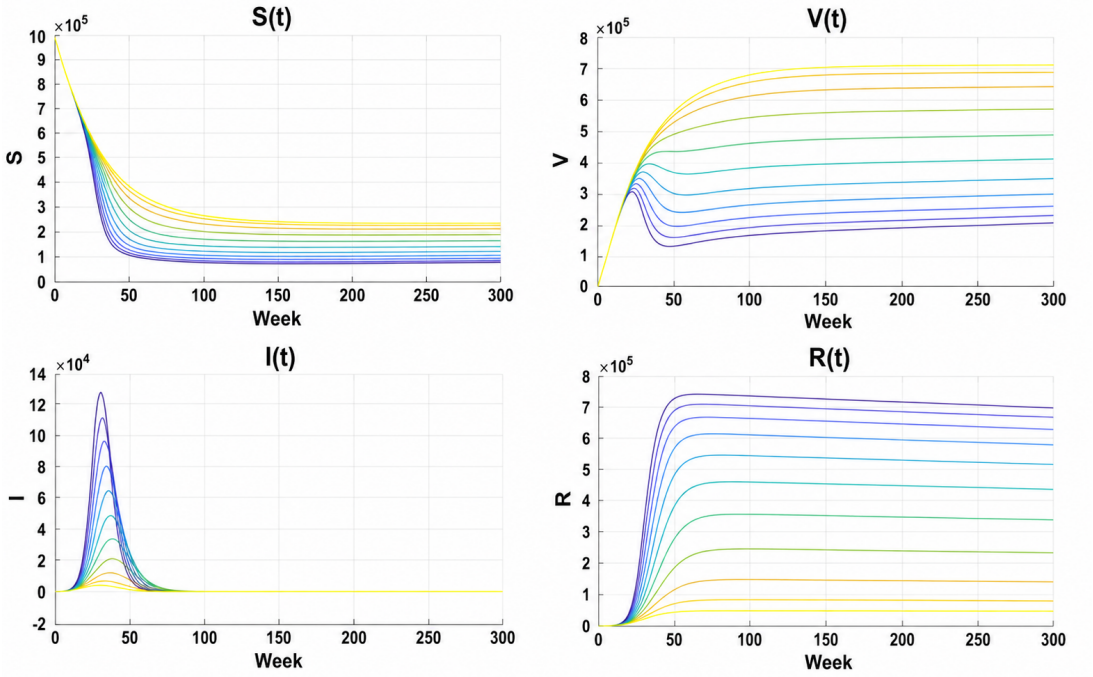

Fig. 8: The effect of variations in ε on the dynamics of the number of infected individuals $I(t)$.

A simultaneous comparison of the curves in Figure 8(i)–(iv), corresponding to $S(t)$, $V(t)$, $I(t)$, and $R(t)$ respectively, clearly shows a monotonically decreasing and consistent pattern across the range of ε values simulated: the higher the vaccine effectiveness value ε, the smaller the value of R_0, and the faster the number of infected individuals $I(t)$ in subplot (iii) decreases toward zero. This pattern aligns with the analytical structure of R_0 in the SVIR model, where ε appears as a reducing factor in the term representing the effective transmission rate in the vaccinated population, so the relationship between ε and R_0 is functionally inverse, consistent with the previously obtained negative sensitivity index.

Furthermore, the results of this analysis identify a critical threshold value for vaccine effectiveness, ε^*, located in the interval $0.5 < \varepsilon^* < 0.75$, which is the minimum value of ε required for the condition $R_0 < 1$ to be satisfied and for the disease to be eliminated from the population. This threshold is further confirmed by three additional simulation scenarios performed for $\varepsilon = 0.5$, 0.75, and 0.8: for $\varepsilon = 0.5$, the infected population $I(t)$ fails to decline toward zero and instead settles at an endemic equilibrium, whereas for $\varepsilon = 0.75$ and $\varepsilon = 0.8$, $I(t)$ progressively approaches zero, indicating that the system has crossed into the disease-free regime. The existence of this threshold has important policy implications: a vaccination program will only be effective in controlling the spread of the disease if the vaccine used has an efficacy rate exceeding ε^*. Below that value, vaccination with any level of coverage cannot bring R_0 below one without additional non-pharmaceutical interventions.

Therefore, the results of this sensitivity analysis confirm that maintaining the quality and integrity of vaccines through proper cold chain management is a top priority in immunization programs. A decline in vaccine effectiveness due to improper handling not only reduces individual protection, but also has the potential to shift the system from a disease-free state to an endemic state overall, as illustrated by the contrast between the $\varepsilon = 0.5$ scenario and the $\varepsilon = 0.75$–0.8 scenarios. In addition, regular monitoring of vaccination coverage is necessary to ensure that the combination of vaccine effectiveness and coverage consistently maintains the R_0 value below one, so that disease elimination can be achieved and sustained in the long term. More importantly, the sharp rise in R_0 when effectiveness drops from 0.85 to 0.75, and even further to 0.5, serves as

a strong warning that vaccine effectiveness must be kept not only above the critical threshold ε^*, but as close as possible to its current high level to maintain a comfortable buffer against epidemic resurgence.

The R_0 values obtained in this study (0.668–1.151) are markedly lower than the classical measles R_0 range of 12–18 reported for fully susceptible populations [24]. This is expected: unlike the classical basic reproduction number, R_0 as derived here (Eq. Eq. (15)) is evaluated at a disease-free equilibrium that already incorporates steady-state vaccination coverage, and is therefore more precisely interpreted as a vaccination-adjusted reproduction number, reflecting the transmission-reducing effect of existing immunization coverage rather than an intrinsically lower transmissibility of measles itself [25]. This context is particularly relevant given that national measles vaccination coverage in Indonesia (approximately 73.46% for children aged 12–23 months) remains well below the 95% threshold typically required for herd immunity, amid a national resurgence exceeding 63,000 suspected cases in 2025–2026 [26].

5. Conclusion

Based on the stability analysis and numerical simulation of the SVIR model regarding the dynamics of measles in Sidoarjo City, East Java, Indonesia, the following conclusions can be drawn:

1. **Equilibrium Points:** The SVIR model with explicit vaccine waning admits a unique endemic equilibrium characterized in closed form (Eq. 29-33), with existence and both local and global stability rigorously tied to R0 via Routh-Hurwitz criteria and Lyapunov function techniques, the latter established under an explicit sufficient condition on the model parameters (Theorem 5).
2. R_0 **and Stability:** Calibration against 2023 Sidoarjo surveillance data via four independent methods identifies PSO as the best-fitting approach (MAPE=10.82%), yielding $R_0 = 0.668$ and confirming the disease-free regime under current conditions.
3. **Numerical Simulation:** The best estimation results using PSO yield $R_0 = 0.668 < 1$, validating that the current situation in Sidoarjo City is disease-free, and the system is converging toward a disease-free state. However, sensitivity simulations with varying vaccine effectiveness reveal a critical pattern: when ε is reduced to 0.75, the basic reproduction number jumps to $R_0 = 0.782$. Although technically still below the epidemic threshold, this value is already very close to $R_0 = 1$, indicating that the system has entered a vulnerable zone. A further decline to $\varepsilon = 0.5$ immediately pushes $R_0 = 1.151 > 1$, making the disease endemic and demonstrating that the system loses its controlled status well before effectiveness drops to that level. Therefore, these results underscore that vaccine effectiveness must be maintained not far below its current high value ($\varepsilon \approx 0.85$); even a moderate decrease to $\varepsilon = 0.75$ brings the population dangerously close to the critical threshold, highlighting the critical importance of preserving vaccine quality and high immunization coverage to prevent a resurgence of measles. These recommendations are derived from a homogeneously mixed population model and therefore represent city-wide guidance; given the sub-district heterogeneity in vaccination coverage that motivated this study, targeted interventions in lower-coverage districts are likely to yield disproportionately larger reductions in transmission risk than uniform city-wide measures — a hypothesis that spatially structured extensions of this model could formally evaluate.
4. **Limitations and Future Works:** This study has several limitations. First, the model assumes a homogeneously mixed population and does not capture sub-district heterogeneity in vaccination coverage, despite motivating evidence of such heterogeneity in Sidoarjo. Second, parameter estimation relies on a single 52-week incidence series without external/out-of-sample validation, raising potential parameter identifiability concerns — particularly for the waning immunity rate σ, whose estimated value (0.0072/week, corresponding to a mean

immunity duration of approximately 2.7 years) is shorter than durations typically reported for two-dose measles immunity; this discrepancy likely reflects data limitations rather than a confirmed biological finding, as σ may be absorbing structural error from unmodeled factors such as primary vaccine failure, cold-chain lapses, or incomplete coverage. Third, sensitivity analysis was restricted to local normalized indices; future work could incorporate global sensitivity methods (e.g., PRCC) to assess parameter interactions. Future research directions include spatially structured or metapopulation extensions, multi-year data validation, and formal identifiability analysis.

CRediT authorship contribution statement

Ainishafa Conceptualization, Methodology, Software, Formal Analysis, Investigation, Data Curation, Writing the Original Draft, Visualization. **Abadi** Conceptualization, Methodology, Validation, Writing Review & Editing, Supervision, Project Administration, Funding Acquisition. **Dian Savitri** Supervision, Writing – Review & Editing.

Declaration of Generative AI and AI-assisted technologies

No generative AI or AI-assisted technologies were used during the preparation of this manuscript.

Declaration of Competing Interest

The authors declare no competing interests.

Funding and Acknowledgments

This research received no external funding.

Data and Code Availability

The data analyzed in this study were sourced from Badan Pusat Statistik (BPS) 2023 for Sidoarjo City, East Java, Indonesia and are publicly accessible at https://sidoarjokab.bps.go.id/. The complete dataset and the MATLAB code are not publicly available, but they can be obtained from the corresponding author upon reasonable request and subject to confidentiality agreements.

References

[1] World Health Organization. “Measles vaccines: WHO position paper”. In: *Weekly Epidemiological Record* 94.6 (2019), pp. 73–96.

[2] Kementerian Kesehatan RI. *Laporan Surveilans Campak dan Rubella Tahunan 2024*. Tech. rep. Jakarta: Kementerian Kesehatan RI, 2024.

[3] M. K. Patel et al. “Progress toward regional measles elimination—worldwide, 2000–2019”. In: *MMWR. Morbidity and Mortality Weekly Report* 69.45 (2020), p. 1700. DOI: 10.15585/mmwr.mm6945a6.

[4] K. M. Thompson, C. L. Odahowski, and J. L. Goodson. “Synthesis of evidence for characterizing measles and rubella immunity and transmission risk”. In: *Risk Analysis* 41.4 (2021), pp. 613–630. DOI: 10.1111/risa.12454.

[5] World Health Organization. *What You Need to Know About Measles*. https://www.who.int/news-room/questions-and-answers/item/what-you-need-to-know-about-measles. Accessed: 2026-07-21. Aug. 2024.

[6] R. M. Anderson and R. M. May. *Infectious Diseases of Humans: Dynamics and Control*. Oxford University Press, 1991.

[7] M. J. Keeling and P. Rohani. *Modeling Infectious Diseases in Humans and Animals*. Princeton University Press, 2011.

[8] W. O. Kermack and A. G. McKendrick. "A contribution to the mathematical theory of epidemics". In: *Proceedings of the Royal Society A* 115.772 (1927), pp. 700–721. DOI: 10.1098/rspa.1927.0118.

[9] D. Aldila et al. "Evaluating vaccination and quarantine for measles intervention strategy in Jakarta, Indonesia through mathematical modeling". In: *Partial Differential Equations in Applied Mathematics* 8.2 (2023), pp. 425–441. DOI: 10.1016/j.padiff.2025.101191.

[10] F. Brauer, C. Castillo-Chavez, and Z. Feng. *Mathematical Models in Epidemiology*. Springer, 2019. DOI: 10.1007/978-1-4939-9828-9.

[11] M. Fakhruddin et al. "Investigation of a measles transmission with vaccination: a case study in Jakarta, Indonesia". In: *Mathematical Biosciences and Engineering* 88.3 (2020), pp. 45–67. DOI: 10.3934/mbe.2020170.

[12] P. van den Driessche. "Reproduction numbers of infectious disease models". In: *Infectious Disease Modelling* 9.1 (2017), pp. 1–12. DOI: 10.1016/j.idm.2017.06.002.

[13] Bo Yang, Zhenhua Yu, and Yuanli Cai. "Global Stability and Optimal Vaccination Control of SVIR Models". In: *AIMS Mathematics* 9.2 (2024), pp. 3453–3482. DOI: 10.3934/math.2024170.

[14] Md Abdul Kuddus, M. Mohiuddin, and Azizur Rahman. "Mathematical Analysis of a Measles Transmission Dynamics Model in Bangladesh with Double Dose Vaccination". In: *Scientific Reports* 11 (2021), p. 16571. DOI: 10.1038/s41598-021-95913-8.

[15] Haileyesus Tessema Alemneh and Molla Admasu Belay. "Modelling, Analysis, and Simulation of Measles Disease Transmission Dynamics". In: *Discrete Dynamics in Nature and Society* 2023 (2023), pp. 1–20. DOI: 10.1155/2023/9353540.

[16] Pauline van den Driessche and James Watmough. "Reproduction Numbers and Subthreshold Endemic Equilibria for Compartmental Models of Disease Transmission". In: *Mathematical Biosciences* 180.1–2 (2002), pp. 29–48. DOI: 10.1016/S0025-5564(02)00108-6.

[17] Miled El Hajji and Amer Hassan Albargi. "A Mathematical Investigation of an "SVEIR" Epidemic Model for the Measles Transmission". In: *Mathematical Biosciences and Engineering* 19.3 (2022), pp. 2853–2875. DOI: 10.3934/mbe.2022131.

[18] Achraf Zinihi, Mostafa Tahiri, and Moulay Rchid Sidi Ammi. "Stability Analysis of a Diffusive SVIR Epidemic Model with Distributed Delay, Imperfect Vaccine and General Incidence Rate". In: *arXiv preprint* (2024). DOI: 10.48550/arXiv.2405.15478.

[19] Rusnanda Rasyad Musafir and Syaiful Anam. "Parameter Estimation of COVID-19 Compartment Model in Indonesia Using Particle Swarm Optimization". In: *Jurnal Berkala Epidemiologi* 10.3 (2022), pp. 283–292. DOI: 10.20473/jbe.V10I32022.283-292.

[20] Maryam A. Alyami et al. "Bayesian Model Selection for COVID-19 Pandemic State Estimation Using Extended Kalman Filters". In: *PLOS Global Public Health* (2024). DOI: 10.1371/journal.pgph.0003467.

[21] Tianyi Li, Hazhir Rahmandad, and John Sterman. "Improving Parameter Estimation of Epidemic Models: Likelihood Functions and Kalman Filtering". In: *SSRN Preprint* (2022). DOI: 10.2139/ssrn.4165188.

[22] Dinas Kesehatan Kabupaten Sidoarjo. *Laporan Surveilans Penyakit Campak Tahunan 2023*. Sidoarjo: Dinkes, 2023.

[23] Badan Pusat Statistik Kabupaten Sidoarjo. *Kecamatan Sidoarjo dalam Angka 2023*. Sidoarjo: BPS, 2023.

[24] F. M. Guerra et al. "The basic reproduction number (R0) of measles: a systematic review". In: *The Lancet Infectious Diseases* 17.12 (2017), e420–e428. DOI: 10.1016/S1473-3099(17)30307-9.

[25] Jacco Wallinga, Daniel Lévy-Bruhl, Nigel J. Gay, and Corien H. Wachmann. "Estimation of measles reproduction ratios and prospects for elimination of measles by vaccination in some Western European countries". In: *Epidemiology and Infection* 127.2 (2001), pp. 281–295. DOI: 10.1017/S095026880100601X.

[26] Erni J. Nelwan. "Measles in Indonesia: Vaccination Coverage and Identified Challenges". In: *Acta Medica Indonesiana* 58.1 (2026). Editorial, p. 3. https://actamedindones.org/index.php/ijim/article/view/3393.